Materials Research Bulletin 137 (2021) 111187

Contents lists available at ScienceDirect

Materials Research Bulletin

journal homepage: www.elsevier.com/locate/matresbu

# Unusual superparamagnetic behavior in bulk $Ba_{0.198}La_{0.784}Ti_{0.096}Fe_{0.8}O_{3-\delta}$

Fatima El Bachraoui [a,b,*], Youssef Tamraoui [a], Said Louihi [b], Jones Alami [a], Reza Shahbazian-Yassar [d], Yifei Yuan [c,d], Khalil Amine [c], Bouchaib Manoun [a,b]

[a] Materials Science and Nano-engineering Department (MSN), University Mohammed VI Polytechnic, Benguerir, Morocco
[b] Hassan First University of Settat, FST, Rayonnement-Matière et Instrumentation, S3M, 26000, Settat, Morocco
[c] Argonne National Lab., Chem Sci & Engn Div, 9700 S Cass Ave, Lemont, IL, 60439, USA
[d] Mechanical and Industrial Engineering, University of Illinois at Chicago, Chicago, IL, 60607, USA

ARTICLE INFO

*Keywords:*
$LaFeO_3$
Magnetic perovskite materials
Superparamagnetic
ZFC-FC
Optical band gap

ABSTRACT

We report the observation of superparamgnetic behavior induced by the substitution $La^{3+}$ by $Ba^{2+}$ at A-sites and $Fe^{+3}$ by $Ti^{4+}$ at B-sites. $Ba_{0.198}La_{0.784}Ti_{0.096}Fe_{0.8}O_{3-\delta}$ was synthesized *via* solid state reaction. The Rietveld refinements revealed an orthorhombic (*Pbnm*). The low-mag STEM results showed that the particles were found to exhibit square like shape and formed in single crystal with high degree of crystallinity. The particle size ranges of 50−300 nm. Element mapping demonstrates a complementary distribution between Ba and La, while homogenous distribution is found for Fe and O. The optical band gap determined from UV–vis analysis is equal to 1.93 eV which is smaller than the reported one for $LaFeO_3$ and $BaTiO_3$. The hysteresis loops at 300 K and 10 K show superparamagnetic behavior, which deviate extremely from the antiferromagnetic nature of $LaFeO_3$ perovskite. The temperature dependent magnetization demonstrates that the material kept a net magnetization of 12.29 (emu/g) at very low temperature.

## 1. Introduction

Superparamgnetism is a phenomenon that appears when the size of magnetic materials particles is less than 150 nm [1]. The magnetic response of the material to the magnetic field results in a steep S-like shape hysteresis loop. Magnetic nanoparticles are regarded as single-domain particles, thus the total magnetic moment of the nanoparticle is considered as one giant magnetic moment [1]. Since the start of the 21st Century, magnetic nano-materials have been the topic of variety of research due to their suitable properties for a broad range of applications such as biomedicine, magnetic ferrofluid catalysis and data storage [2–4], *etc*. Among the most studied magnetic nanomaterials, $Fe_3O_4$ is an important class of half metallic materials, their utilization in the field of biomedicine has been the topic of several studies [2]. However, because of their ability to get oxidized easily due to the nature of its structure, and to the requirement of optimizing several parameters [5], introducing new type of materials will overcome this problem. Several researches are focused now on producing magnetic nanomaterials based on perovskite structure. Owing to their flexible structure and their ability to accommodate a wide range of periodic table elements, perovskite materials are considered as a suitable target for physical property development [6,7]. This class of materials is described with the general formula ($ABO_3$), where A is a rare or alkaline earth element and B is a transition metal cation. One great feature of these types of materials is their extremely thermodynamically stable atomic arrangement. The orthoferrite perovskite family $AFeO_3$ (A = La, Lu, Er, Sm, *etc*.) are reported to be weak ferromagnetic showing bewildering magneto-optical properties [8,9]. In particular, lanthanum iron oxide $LaFeO_3$ is one of the most studied perovskite-type material, it crystallizes in an orthorhombically distorted structure with *Pbnm* space group (no. 62) showing multiferroicity in a single phase [10,11]. $LaFeO_3$ is found to be a G-type antiferromagnetic material with high Neel temperature $T_N$=480 °C, and shows a ferroelectric transition around 200 °C [10,12]. The origin of antiferromagnetic in $LaFeO_3$ is due to the $Fe^{3+}$ anti-parallel spin interaction nature between two sub-lattices (superexchange reactions) which results in a small net magnetization [13,14], it should be noted that this property can be shaped depending on the nature of (A-Fe) exchange interaction, the stoichiometry, oxygen vacancies and temperature. Recently more attention is paid to decreasing the particle size of $LaFeO_3$ in order to improve the magnetic property at room temperature [15,16]. The magnetization of the sample increases with decreasing particle size and a shift of Curie temperature is observed ($T_c$)

* Corresponding author at: Materials Science and Nano-engineering Department (MSN), University Mohammed VI polytechnic, Benguerir, Morocco.
*E-mail address:* fatima.elbachraoui@um6p.ma (F. El Bachraoui).

https://doi.org/10.1016/j.materresbull.2020.111187
Received 8 October 2020; Received in revised form 11 December 2020; Accepted 16 December 2020
Available online 29 December 2020

[17,18]. At present, various type of substitution have been investigated, in the reported work $LaFe_{1-x}Zn_xO_3$ ($0 < x < 0,3$), the substitution of Fe by Zn has shown a weak ferromagnetic response of all doped samples [19]. In another work where Fe was substituted by Mn, $LaFe_{1-x}Mn_xO_3$, the coercivity has decreased from 632 to 190 Oe, reporting an enhancement of the magnetic moment and a control over the coercive field from the antiferromagnetic $LaFeO_3$ [20]. The creation of ions of mixed valency was investigated in $LaFeO_3$ doped Ag and was found to increase the susceptibility at a specific temperature [21]. In A-site substitution of La by Al in $La_{0.5}Al_{0.5}FeO_3$, the magnetization and the susceptibility have both considerably enhanced [22]. Change in the magnetic property of $LaFeO_3$ at the nano-scale was also studied, and it was found that $LaFeO_3$ nanoparticles with an average diameter of 16 nm exhibit superparamagnetic behavior and with increasing the grain size, the particles exhibit the exchange bias properties at around 22 nm [17, 18]. It should be noted that the superparamgnetism Phenomenon in Materials is generally due the reduced size of particles. On the Other hand $BaTiO_3$ perovskite is known to show high dielectric constant and has been the topic of numerous works [23]. $BaTiO_3$ has also been tested for photocatalysts applications [24]. The synthesis of solid solutions combining different elements produces multifunctional materials, as it can also enhance or not a specific property of the hosting material. Up to now, there was no work reporting substitution inducing a superparamagnetic response in $LaFeO_3$. In the same aim of enhancing $LaFeO_3$ magnetic property, we report in this work the structural, morphology, optical and magnetic properties of the prepared $Ba_{0.198}La_{0.784}Ti_{0.096}Fe_{0.8}O_{3-\delta}$ *via* the conventional solid state reaction method.

## 2. Experimental

### 2.1. Sample preparation

The perovskite sample $Ba_{0.198}La_{0.784}Ti_{0.096}Fe_{0.8}O_{3-\delta}$ was synthesized *via* the conventional solid state reaction method. The starting materials, $BaCO_3$, $La_2O_3$, $TiO_2$ and $Fe_2O_3$ of 99.9 % purity were well mixed and ground in an agate mortar and heated in air, in alumina crucible, at progressively higher temperature (600 °C, 800 °C, 1000 °C) overnight with periodic intermediate regrinding. The chemical reaction is:

$$0.2\ BaCO_3 + 0.4\ Fe_2O_3 + 0.4\ La_2O_3 + 0.1TiO_2 \rightarrow (0.99)\ Ba_{0.198}La_{0.784}Ti_{0.096}Fe_{0.8}O_{3-\delta} + (0.01)\ BaLa_2Ti_4O_{12} + 0.2CO_2^{\uparrow}$$

The obtained product $Ba_{0.198}La_{0.784}Ti_{0.096}Fe_{0.8}O_{3-\delta}$ was characterized by X-ray diffraction, low quantities of impurity $BaLa_2Ti_4O_{12}$ was observed in the patterns. For UV–vis measurements of the diffuse reflectance, 0.5 g of the resulting powder was used and was pressed into pellet in the presence of a binder poly(vinylalcohol) (PVA) using a steel die of 1 mm diameter in an hydraulic press under a pressure of 6 t. The pellet of 0.5 mm thickness and 1 mm diameter was sintered in air at 900 °C for 8 h.

### 2.2. XRD measurements

At room temperature, the X-ray powder diffraction data were collected on a D2 PHASER diffractometer, with the bragg-brentano geometry (CuKα radiation, $\lambda = 1.5406$ Å) at 30 KV and 10 mA. The pattern was scanned in steps of 0.01 (2θ) in the range $15 < 2\theta < 105°$, time step = 0.3 s/step.

The full pattern refinements were performed by means of the Rietveld method using the Fullprof program [25] integrated in Winplotr software [26]. The Rietveld refinement of the observed XRD data was initiated with scale parameter, the background of the X-ray diffraction pattern is fitted with a fifth order polynomial. Successively, other profile parameters are added. The peak shape was adjusted with a pseudo-voigt profile function. The parameters positions and isotropic atomic displacement of individual atoms were further refined.

### 2.3. UV–vis measurements

Using a PerkinElmer UV/VIS/NIR spectrometer Lambda 1050, the UV–vis diffuse reflectance spectra were recorded at room temperature in the range of 250−800 nm, a homemade support was used to hold the sample during the measurements.

### 2.4. Magnetic measurements

Magnetization measurements were carried out using a superconducting quantum interference device (SQUID) magnetometer MPMS (Magnetic Property Measurement System). The hysteresis loop ((M-H)) was taken at 300 K and 10 K with magnetic field cycling between -80 KOe and +80 KOe. Under field cooled (FC) and zero field cooled (ZFC) condition, the temperature dependent magnetic moments profile was measured in the temperature range of 5 K–350 K under an applied magnetic field of 500 Oe.

### 2.5. Morphology and atomic structure

The STEM-ABF and HAADF measurements were done using an aberration-corrected JEOL ARM200CF equipped with a 200 keV cold-field emission gun, annular bright field (ABF) and high angle annular dark field (HAADF) detectors, and an energy dispersive spectrometer (EDS). 22 mrad probe convergence angle was used for all the images and spectra.

## 3. Results and discussion

### 3.1. Structure determination and description

The X-ray diffraction analysis at room temperature confirms the formation of the desired crystalline structure. The patterns of the prepared compound $Ba_{0.198}La_{0.784}Ti_{0.096}Fe_{0.8}O_{3-\delta}$ indicate a perovskite structure. Reflections of $Ba_{0.198}La_{0.784}Ti_{0.096}Fe_{0.8}O_{3-\delta}$ perovskite patterns were indexed by means of the computer program Dicvol [26] on the basis of an orthorhombic simple perovskite unit cell with the space group *Pbnm* (no. 62). The first 15 peak positions, with a maximal absolute error of 0.03° (2θ), were used as input data. The characteristic peaks for $Ba_{0.198}La_{0.784}Ti_{0.096}Fe_{0.8}O_{3-\delta}$ is located at $2\theta = 32.17°$ and it corresponds to (200), (112) and (020) planes of the crystal structure. The Rietveld Refinement analysis was carried out using FullProf program coupled with Wintplotr software. The initial structure used for the refinement is based on the model of $LaFeO_3$ reported in [27]. At 25.96°, 29.54° and 31.22° appears to be part of $BaLa_2Ti_4O_{12}$ impurities. Fig. 1 displays the observed and calculated X-ray diffraction patterns. Along with the secondary phase, refinement with this model yields to satisfactory agreement factors with reliability factors of $R_p = 5.04$, $Rw_p = 7.38$ and $\chi^2 = 2.29$. The refinement results of the structural and instrumental parameters of $Ba_{0.198}La_{0.784}Ti_{0.096}Fe_{0.8}O_{3-\delta}$ simple perovskite are summarized in Table 1.

### 3.2. Morphology and atomic structure

Fig. 2**(a, d)** displays the low-mag STEM images of a few perovskite $Ba_{0.198}La_{0.784}Ti_{0.096}Fe_{0.8}O_{3-\delta}$ particles, where the particle size is seen to be in the range of 50−300 nm featuring certain degree of particle aggregation. Additionally, the as-synthesized particles are formed in squared like shapes as presented in Fig. 2**(a, d)**. The compositional analyses in Fig. 2**(b, e)** showed that La:Fe:Ba ratio is close to the chemical formula of the composition (*i.e.* 4:1:1), while Ti was hardly detected due to its limited amount in the sample. The elemental mapping results show that while Fe and O are uniformly distributed within a single particle, Ba and La are not as uniform but exhibit a certain degree of local inhomogeneity, which interestingly demonstrated mutually complementary distribution. The EELS analysis in Fig. 2**(c)** further confirmed that

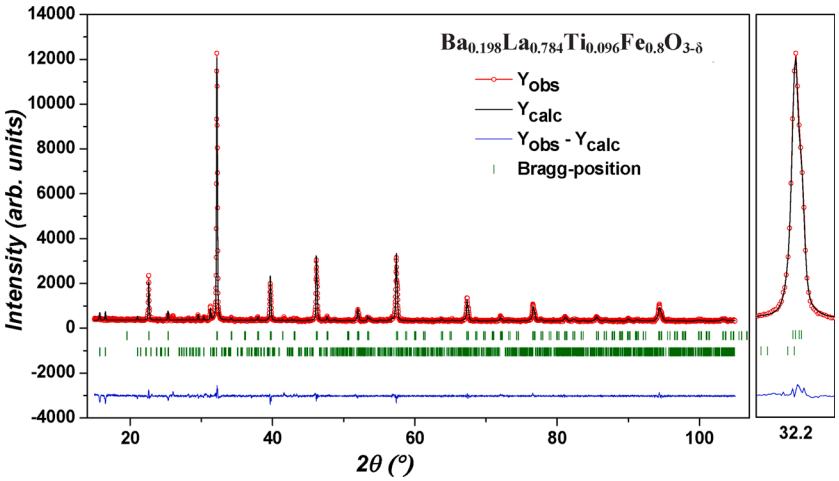


**Fig. 1.** Final Rietveld Refinement plots of Orthorhombic $Ba_{0.198}La_{0.784}Ti_{0.096}Fe_{0.8}O_{3-\delta}$, perovskites samples. The observed data and calculated profile are indicated by circles and solid trace respectively. The lowest trace shows the difference between the observed and calculated model. The vertical bars indicate the calculated bragg reflections positions.

**Table 1**
Refined structural parameters for $Ba_{0.198}La_{0.784}Ti_{0.096}Fe_{0.8}O_{3-\delta}$.

| atom | x | y | z | B(Å$^2$) | occupancy |
|---|---|---|---|---|---|
| Ba | −0.0093 (7) | 0.0233(4) | 1/4 | 0.72(2) | 0.198 |
| La | −0.0093(7) | 0.0233(4) | 1/4 | 0.72(2) | 0.784 |
| Ti | 0 | 1/2 | 0 | 0.94(5) | 0.096 |
| Fe | 0 | 1/2 | 0 | 0.94(5) | 0.8 |
| O1 | 0.068(7) | 0.486(3) | 1/2 | 0.99(1) | 1.0 |
| O2 | −0.322(4) | 0.237(5) | 0.020(4) | 0.99(1) | 1.766 |
| Space group: *Pbnm* (orthorhombic) | | | | | |
| Cell parameters | | | | | |
| a = 5.5619 (5) (Å) b = 5.5557 (4) (Å) c = 7.8553 (1) (Å) α=β=γ = 90° | | | | | |
| Cell Volume: 242.733(3) (Å)$^3$ | | | | | |
| Caglioti parameters: U = 0.0757 (7) V = −0.0292 (6) W = 0.0119 (1) | | | | | |
| Reliability Factors | $\chi^2$: 1.65; Rp: 4.76; Rwp: 6.26; Rexp: 4.87; $R_B$: 7.17 | | | | |

Wavelength (Å): λkα1 = 1.5406, 2θrange (°): 15–105, Step scan increment (°2θ), Program: FULLPROF.

there is a very limited quantity of Ti while Fe, Ba, La and O are present in the sample with strong signals. The ABF and HAADF images in Fig. 2**(f)** demonstrate the atomic structure of a single particle, indicating its single-crystalline property with a high degree of crystallinity.

### 3.3. Optical measurement and band gap determination

Fig. 3**(b)** illustrates the UV–vis absorbance spectrum of $Ba_{0.198}La_{0.784}Ti_{0.096}Fe_{0.8}O_{3-\delta}$. The new synthesized perovskite shows a strong absorbance response in the ultraviolet (~ 250−400 nm) and the visible light region (~ 400−800 nm). The optical response in the visible light region makes the sample an interesting candidate as visible light photocatalyst. To estimate the optical band gap energy of $Ba_{0.198}La_{0.784}Ti_{0.096}Fe_{0.8}O_{3-\delta}$, Kubelka-Munk theory was used to analyze the reflectance spectra which was converted in accordance with the following equation: $F(R) \equiv \alpha/s = (1-R)^2/2R$ (eq.1), where R is the reflectance, F(R) is the Kubelka-Munk function, $\alpha$ is the absorption coefficient which is proportional to F(R) and $s$ is the scattering factor, in some cases S is approximately equal to unity or it is a constant [28,29]. The optical band gap or the energy dependence near absorption edge can be determined according to tauc's plot equation [30]: $\alpha h\nu = A(h\nu - E_g)^n$ where A is an energy-independent constant related to the effective mass of electrons and holes and $E_g$ is the optical band gap. Hence **eq.1** can be written as: $F(R)h\nu = A(h\nu - E_g)^n$. The exponent n depends on the inter-band transition mechanism and it is a characteristic of the transition type: n = 1/2, 2, 3/2 and 3 respectively for direct allowed transitions, indirect allowed transition, direct forbidden transitions and indirect forbidden transitions. In the case of the indirect forbidden transitions n = 3, which was the best choice for this case, $(F(R)h\nu)^3$ *versus* $h\nu$ should give a straight line near the absorption edge. The intersection of the straight line fitting with $h\nu$ where the absorption is equal to zero F(R) → 0 gives the value of $E_g$ as an example shown in the inset in Fig. 3**(a).** The estimated band gap of the sample is equal to 1.93 eV. Such results suggest good conductivity properties of this material and make it good candidate for solid oxide fuel cell cathode, as it can cause also high photo-catalytic activity. The small band gap value obtained can be explained as follow: both structural parameters and the composition are factors that have an influence on the optical band gap value. The band gap in perovskite materials is B-O-B dependent, it is reported that samples with a bond angle close to 180° tend to have a smaller band gap [31,32], in our case $Fe^{3+}/Ti^{4+}$-$O_1$-$Fe^{3+}/Ti^{4+}$ and $Fe^{3+}/Ti^{4+}$-$O_2$-$Fe^{3+}/Ti^{4+}$ are equal to 154.04° and 167.523° respectively. Moreover, the conduction band is constituted by elements at the B-site of the perovskite structure, while O2p are responsible for the valence band. Thus, having $Ti^{4+}$ / $Fe^{3+}$ at the B-site may induce a shift of the conduction band resulting in a shrink of the optical band gap [33].

### 3.4. Magnetic measurements

The magnetization variation curve as function of the applied magnetic field M (H) recorded at 300 K and 10 K are illustrated in Fig. 4**(a)** and **(b)** respectively. The (M-H) hysteresis loop reflects the magnetic response of the prepared perovskite $Ba_{0.198}La_{0.784}Ti_{0.096}Fe_{0.8}O_{3-\boldsymbol{\delta}}$ to the external applied field, and gives information about the magnetic type behavior. At 300 K, the sample shows a steep and very narrow hysteresis in the form of an S like shape and reaches a maximum of $M_s/\mu_B = 0.49$ known as the magnetization saturation, which was evaluated according to the law of approach to saturation by the extrapolation of the magnetization *versus* 1/H to 1/H → 0 [30]. The very negligible values of the coercivity $H_c = 17$ Oe, and the remanence $M_r/\mu_B = 0.78$ indicate a superparamagnetic behavior at 300 K [34]. The very low value of squareness factor SQ = Mr/Ms = 1.59 and the steep initial slope in the magnetization curve are feature suggesting the presence of pseudo-single domain and confirming the superparamagnetic behavior [35]. In fact, many factors can alter the M (H) hysteresis loop curve such as the crystallite size distributions, anisotropy and the interaction of identical particles. Therefore, experimentally the absence of the hysteresis loop resulting in a very small coercivity (few Oersted) and negligible remanence $M_r$~0 were found for ferro/ferromagnetic

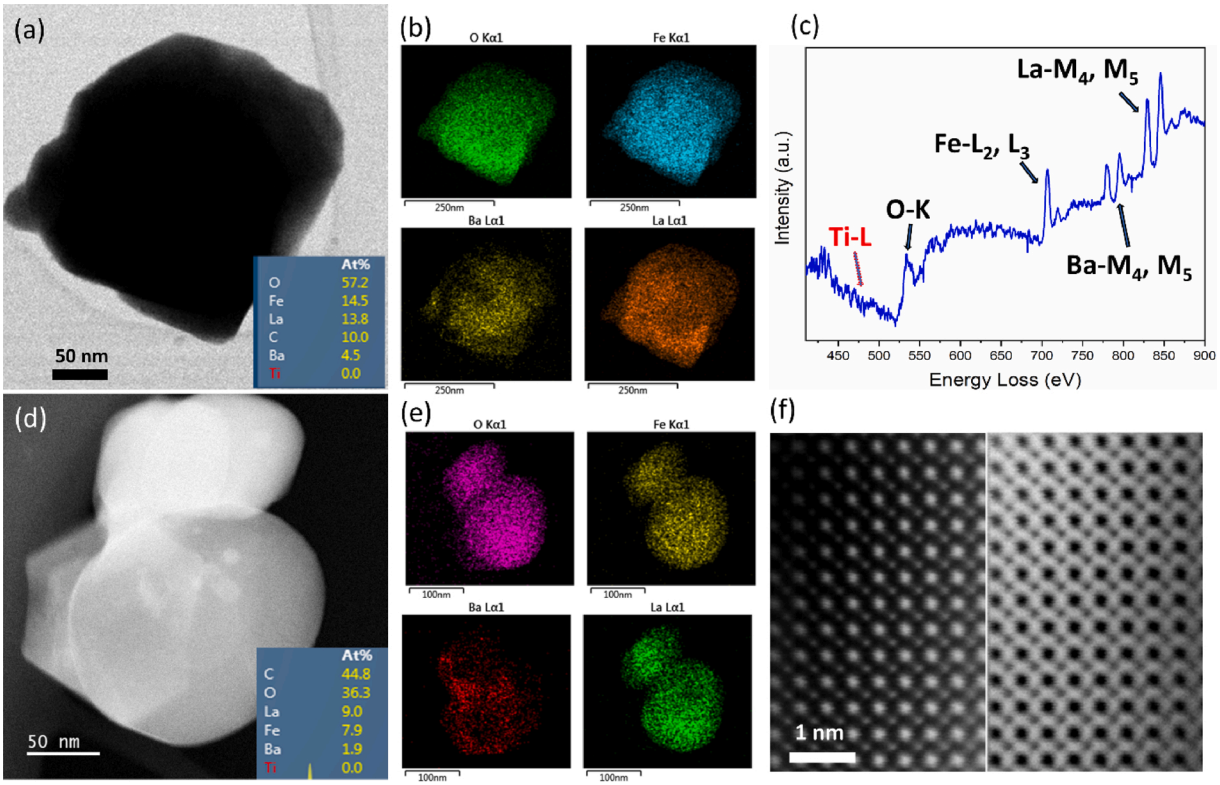


**Fig. 2.** Representative ABF and HAADF STEM images (a, d), corresponding compositional analyses ((b, e) for EDS mapping and (c) for electron energy loss spectroscopy) and the ABF and HAADF atomic structure study (f) of the perovskite sample $Ba_{0.198}La_{0.784}Ti_{0.096}Fe_{0.8}O_{3-\delta}$.

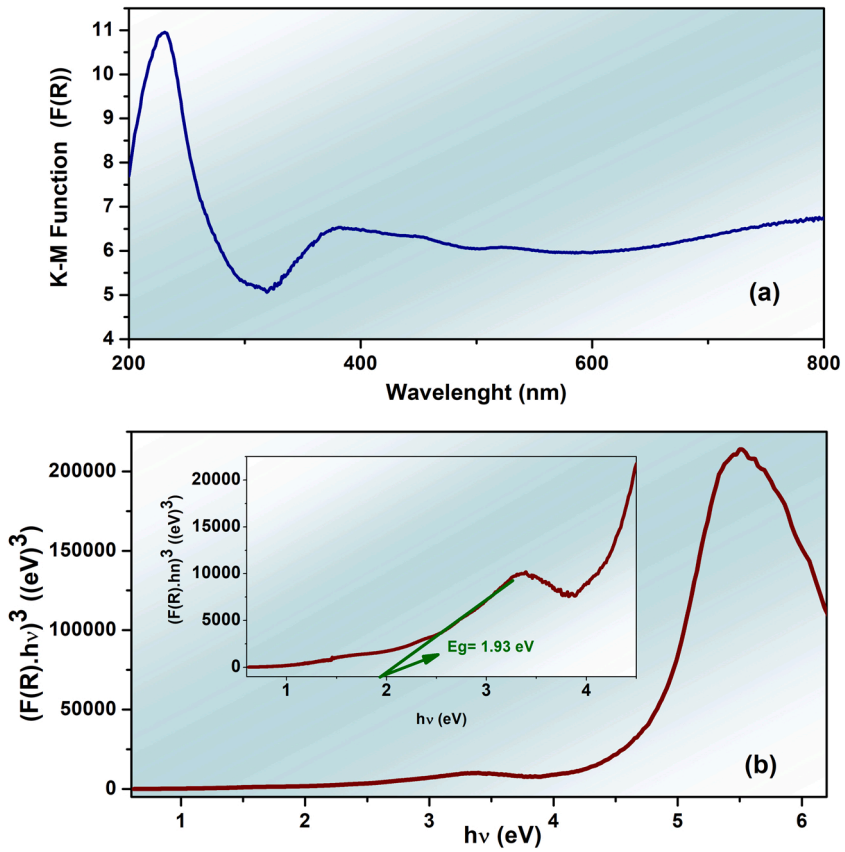


**Fig. 3.** (Fig. 2**(a))** Dependence of $(F(R)*h\nu)^3$ of the Orthorhombic $Ba_{0.198}La_{0.784}Ti_{0.096}Fe_{0.8}O_{3-\delta}$ perovskite sample upon the incident photon energy ($h\nu$). (Fig. 2**(b))** UV–vis Spectra showing the evolution of absorption coefficient (K-M function) in the range of wavelength between 200 and 800 nm.

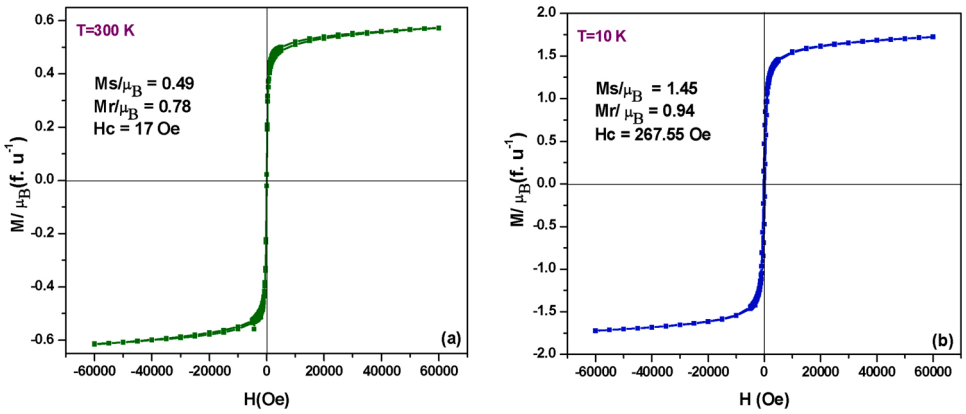


**Fig. 4.** M–H curve measured in the range of the magnetic field ±60 kOe at 300 K (Fig. 3**(a)**) and 10 K (Fig. 3**(b)**) of $Ba_{0.198}La_{0.784}Ti_{0.096}Fe_{0.8}O_{3-\delta}$.

nanoparticles below certain size which in turn can behave as superparamagnetic nanoparticles and show a very narrow hysteresis loop [35]. Despite the very low coercivity value (equal or close to zero) superparamagnetic system is known to have high heating efficiency. At 10 K, the magnetic response of the perovskite material $Ba_{0.198}La_{0.784}Ti_{0.096}Fe_{0.8}O_{3-\delta}$ to the applied field shows higher magnetization saturation value of $M_s/\mu_B = 1.45$. Other distinct features are the coercivity and the remanences which are systematically higher than those measured at 300 K due to the thermal fluctuations of the magnetic moments at higher temperatures [36]. The coercivity and remanence show values of $H_c = 267.55$ Oe and $M_r/\mu_B = 0.94$, respectively and a squareness factor equal to SQ = 0.33. These observations related to the hysteresis loop demonstrate that the material behavior in its fundamental state is a superparamagnetic. The squareness coefficient was found to be smaller than the theoretical value SQ = 0.5 which indicates that particles are single-domain [35]. To study the temperature dependent magnetization M(T) for the prepared sample $Ba_{0.198}La_{0.784}Ti_{0.096}Fe_{0.8}O_{3-\delta}$, Zero Field Cooling (ZFC) and Field Cooling (FC) measurements were performed between 5 K and 300 K at a fixed magnetic field of 500 Oe, Fig. 5**(a)**. In spite the fact that M (H) measurement at 300 K are sufficient to conclude the magnetic behavior of the material; the ZFC and FC magnetization *versus* temperature M (T) give additional information on magnetic behavior such as Curie temperature ($T_c$) and the blocking temperature which is a characteristic of the equilibrium between the thermal energy ($K_BT_B$) and the anisotropy energy barrier $E_a = K_{eff}V$ where $K_B$, $K_{eff}$ and V represent the Boltzmann constant, anisotropy energy density and the particle volume respectively. At ZFC mode when the sample is cooled down from 300 K to very low temperature 5k the magnetization increases to reach a maximum corresponding to the blocking temperature $T_B = 151.43$ K followed by a continuous decrease while that of FC decreases while increasing the temperature from 5 K to 300 K. Following the behavior of the magnetization *versus* temperature, ZFC and FC above the blocking temperature show a similar behavior, and below it, they significantly split and take different trends, this irreversibility is a characteristic of the blocking-unblocking process of the magnetic particles as the thermal energy changes. At low temperature 5 K the material keeps a net magnetization equal to $M/\mu_B = 4.12$. This meaning that some of the magnetic particles keep aligned leading to a non-zero net magnetization. Below the blocking temperature the relaxation time of the magnetic particles increases and the magnetic moments of the particles are blocked, at $T_B$ the thermal energy and the energy of aligned moments are comparable, as the temperature arises above $T_B$ it leads to a decrement of the magnetization due to the disorientation of the aligned moment caused by the thermal energy. When applying the external field at low temperature, the randomly oriented moments begin to align in the direction of the field, as the temperature increases the magnetization decreases due to the thermal fluctuation of the magnetic moments caused by the thermal energy. Hence, the variation of the magnetization in ZFC and FC process indicates a superparamagnetic behavior.

## 4. Conclusion

$Ba_{0.198}La_{0.784}Ti_{0.096}Fe_{0.8}O_{3-\delta}$ solid solution was successfully synthesized through the conventional solid state reaction method. The substitution as observed influences the structural, optical and magnetic properties. Using the Rietveld refinement, the system was found to crystalize in an orthorhombic system with *Pbnm*, the cell parameters and bond angles were found to be different from those of $LaFeO_3$. the low-mag STEM images shows that the particles are formed in squared like shapes with size ranging between 50−300 nm featuring certain degree of aggregation. The Ti was hardly detected while that of La:Fe:Ba ration is close to the chemical formula as demonstrated by the compositional analysis. Uniformity of the elements was studied, the element mapping

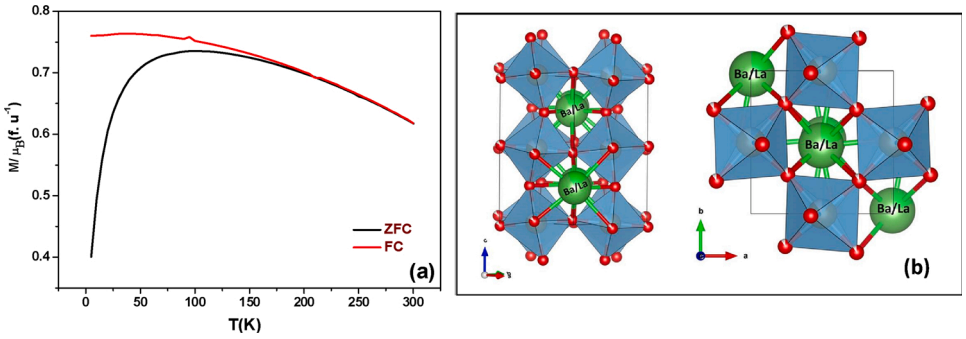


**Fig. 5.** M–T curve in temperature range of 4K-300 K measured at 500 Oe of$Ba_{0.198}La_{0.784}Ti_{0.096}Fe_{0.8}O_{3-\delta}$perovskite sample (Fig. 4(a)). The projection of the unit cell structure of the $Ba_{0.198}La_{0.784}Ti_{0.096}Fe_{0.8}O_{3-\delta}$ unit cell illustrating the typical polyhedral arrangement and the tilt pattern (Fig. 4(b)).

results showed a local inhomogeneity for Ba and La while Fe and O were uniformly distributed with a single particle. Despite the inhomogeneity between Ba and La they demonstrated mutual complementary distribution. The ABF and HAADF results demonstrated the atomic structure of single particles with high degree of crystallinity which is in good agreement with the XRD results. The band gap calculated using tauc plot method was found to be 1.93 eV, in which, the prepared material exhibits an indirect forbidden transition band gap type and the effect of the substitution was reflected in a narrowed band gap. The effect of the substitution in the G-canted type antifferomagnetic $LaFeO_3$, has induced superparamgnetism. At room temperature the hyseresis loop M(H) of the prepared material show a nonlinear behavior of the magnetization *versus* the applied field and shows a steep and narrow hysteresis loop reaching a magnetization saturation of $M_s/\mu_B = 0.49$, the small value of $H_c = 17$ Oe, $M_r/\mu_B = 0.78$ emu/g and SQ = Mr/Ms = 1.59 are features of a superparamagnetic behavior, which was also confirmed by the ZFC-FC irreversibility behavior and the broad peak observed while increasing the temperature, the blocking temperature is $T_B = 151.43$ K. At 5 K, the material keeps a net magnetization equal to $M/\mu_B = 4.12$ concluded from the ZFC curve which was in agreement with the hysteresis loop showing higher saturation magnetization $M_s/\mu_B = 1.45$. The coercivity and remanence show values of $H_c = 267.55$ Oe and $M_r/\mu_B = 0.94$. These results demonstrate the great influence of a precisely percentage implementation of $BaTiO_3$ into $LaFeO_3$, leading to a decrease in the particle size and thus the observation of superparamagnetic feature.

## CRediT authorship contribution statement

**Fatima El Bachraoui:** Writing - original draft, Writing - review & editing, Conceptualization, Methodology, Investigation. **Youssef Tamraoui:** Supervision, Conceptualization, Methodology, Validation, Writing - review & editing. **Said Louihi:** Visualization, Writing - review & editing. **Jones Alami:** Writing - review & editing, Conceptualization, Methodology, Validation. **Reza Shahbazian-Yassar:** Writing - review & editing, Investigation. **Yifei Yuan:** Writing - review & editing, Investigation. **Khalil Amine:** Writing - review & editing, Investigation, Validation. **Bouchaib Manoun:** Supervision, Conceptualization, Methodology, Writing - review & editing, Validation.

## Declaration of Competing Interest

The authors report no declarations of interest.

## Acknowledgments

The authors are grateful to Mohammed VI Polytechnic University, the Office Chérifien des Phosphates in the Moroccan Kingdom (OCP group) and University Hassan 1 st for their suppor and MAScIR foundation for the magnetic measurements. This work made use of instruments in the Electron Microscopy Service (Research Resources Center, UIC). Y.Y. and R.S.Y. acknowledge the funding from NSFDMR-1809439. Y.Y. acknowledges funding from the Argonne National Laboratory-University of Illinois at Chicago subcontract (no. 4J-30361).

## References

[1] G.A.O. Jinhao, G.U. Hongwei, X.U. Bing, Multifunctional magnetic nanoparticles: design, synthesis, and biomedical applications, Acc. Chem. Res. 42 (2009) 1097–1107, https://doi.org/10.1021/ar9000026.
[2] K. Zhu, Y. Ju, J. Xu, et al., Magnetic nanomaterials: chemical design, synthesis, and potential applications, Acc. Chem. Res. 51 (2018) 404–413, https://doi.org/10.1021/acs.accounts.7b00407.
[3] R.B. Nasir Baig, M.N. Nadagouda, R.S. Varma, Magnetically retrievable catalysts for asymmetric synthesis, Coord. Chem. Rev. 287 (2015) 137–156.
[4] A.C. Gandhi, S.Y. Wu, Unidirectional anisotropy mediated giant memory effect in antiferromagnetic Cr2O3 nanorods, RSC Adv. 7 (2017) 25512–25518, https://doi.org/10.1039/c7ra03934d.
[5] A.K. Singh, O.N. Srivastava, A.K. Singh, Shape and size-dependent magnetic properties of Fe3O4 nanoparticles synthesized using piperidine, Nanoscale Res. Lett. 12 (298) (2017).
[6] Y. Tamraoui, B. Manoun, F. Mirinioui, et al., Temperature and composition induced phase transitions in Sr2−xCa1+xTeO6 ($0 \leq x \leq 2$) double perovskite oxides, J. Mol. Struct. 1131 (2017) 103–113, https://doi.org/10.1016/j.molstruc.2016.11.036.
[7] H. Bih, L. Bih, B. Manoun, et al., Raman spectroscopic study of the phase transitions sequence in Li3Fe2(PO4)3 and Na3Fe2(PO4)3 at high temperature, J. Mol. Struct. 936 (2009) 147–155, https://doi.org/10.1016/j.molstruc.2009.07.035.
[8] L.T. Tsymbal, Y.B. Bazaliy, V.N. Derkachenko, et al., Magnetic and structural properties of spin-reorientation transitions in orthoferrites, J. Appl. Phys. 101 (2007), 123919, https://doi.org/10.1063/1.2749404.
[9] R.L. White, Review of recent work on the magnetic and spectroscopic properties of the rare-earth orthoferrites, J. Appl. Phys. 40 (1969) 1061–1069, https://doi.org/10.1063/1.1657530.
[10] P. Jain, S. Srivastava, Investigation of structural, magnetic and electrical properties of pure LaFeO 3 synthesized through solution combustion technique, Digest Journal of Nanomaterials and Biostructures 10 (1) (2015) 141–147.
[11] M. Etter, M. Müller, M. Hanfland, et al., High-pressure phase transitions in the rare-earth orthoferrite LaFeO 3, Acta Crystallogr. Sect. B Struct. Sci. Cryst. Eng. Mater. 70 (2014) 452–458, https://doi.org/10.1107/S2052520614007379.
[12] F. Nolting, A. Scholl, J. Stöhr, et al., Direct observation of the alignment of ferromagnetic spins by antiferromagnetic spins, Nature 405 (2000) 767–769, https://doi.org/10.1038/35015515.
[13] S. Phokha, S. Pinitsoontorn, S. Rujirawat, S. Maensiri, Polymerized complex synthesis and effect of Ti dopant on magnetic properties of LaFeO&SUB&3&/SUB& nanoparticles, J. Nanosci. Nanotechnol. 15 (2015) 9171–9177, https://doi.org/10.1166/jnn.2015.11407.
[14] R.H. Kodama, A.E. Berkowitz, Atomic-scale magnetic modeling of oxide nanoparticles, Phys. Rev. B 59 (1999) 6321–6336, https://doi.org/10.1103/PhysRevB.59.6321.
[15] X. Yu, X. An, Enhanced magnetic and optical properties of pure and (Mn, Sr) doped BiFeO3 nanocrystals, Solid State Commun. 149 (2009) 711–714, https://doi.org/10.1016/J.SSC.2009.02.010.
[16] Tae-Jin Park, Georgia C. Papaefthymiou, Arthur J. Viescas, et al., Size-Dependent Magnetic Properties of Single-Crystalline Multiferroic BiFeO3 Nanoparticles, 2007, https://doi.org/10.1021/NL063039W.
[17] C. Sasikala, N. Durairaj, I. Baskaran, et al., Transition metal titanium (Ti) doped LaFeO3 nanoparticles for enhanced optical structural and magnetic properties, J. Alloys Compd. 712 (2017) 870–877, https://doi.org/10.1016/j.jallcom.2017.04.133.
[18] H. Ahmadvand, H. Salamati, P. Kameli, et al., Exchange bias in LaFeO3 nanoparticles, J. Phys. D Appl. Phys. 43 (2010), https://doi.org/10.1088/0022-3727/43/24/245002.
[19] I. Bhat, S. Husain, W. Khan, S.I. Patil, Effect of Zn doping on structural, magnetic and dielectric properties of LaFeO3 synthesized through sol-gel auto-combustion process, Mater. Res. Bull. 48 (2013) 4506–4512, https://doi.org/10.1016/j.materresbull.2013.07.028.
[20] J.H. Jeong, C.G. Song, K.H. Kim, et al., Effect of Mn doping on particulate size and magnetic properties of LaFeO3nanofiber synthesized by electrospinning, J. Alloys Compd. 749 (2018) 599–604, https://doi.org/10.1016/j.jallcom.2018.03.352.
[21] M.B. Bellakki, B.J. Kelly, V. Manivannan, Synthesis, characterization, and property studies of (La, Ag) FeO3($0.0 \leq x \leq 0.3$) perovskites, J. Alloys Compd. 489 (2010) 64–71, https://doi.org/10.1016/j.jallcom.2009.08.059.
[22] S. Acharya, P.K. Chakrabarti, Some interesting observations on the magnetic and electric properties of Al3+doped lanthanum orthoferrite (La0.5Al0.5FeO3), Solid State Commun. 150 (2010) 1234–1237, https://doi.org/10.1016/j.ssc.2010.04.006.
[23] Z. Chchiyai, F. El Bachraoui, Y. Tamraoui, et al., Design and characterization of novel manganite perovskites Ba1-xBixTi1-xMnxO3 ($0 \leq x \leq 0.2$), Ceram. Int. (2020), https://doi.org/10.1016/j.ceramint.2020.07.169.
[24] Ö Küçük, S. Teber, İ Cihan Kaya, et al., Photocatalytic activity and dielectric properties of hydrothermally derived tetragonal BaTiO3 nanoparticles using TiO2 nanofibers, J. Alloys Compd. 765 (2018) 82–91, https://doi.org/10.1016/j.jallcom.2018.06.165.
[25] J. Rodríguez-Carvajal, ) FULLPROF: a program for rietveld refinement and pattern matching analysis. Abstracts of the Satellite Meeting on Powder Diffraction of the XV Congress of the IUCr, 1990.
[26] T. Roisnel, J. Rodríquez-Carvajal, WinPLOTR: A windows tool for powder diffraction pattern analysis, Mater. Sci. Forum 378–381 (2001) 118–123.
[27] M. Etter, M. Müller, M. Hanfland, R.E. Dinnebier, High-pressure phase transitions in the rare-earth orthoferrite LaFeO3, Acta Crystallogr. Sect. B Struct. Sci. Cryst. Eng. Mater. 70 (2014) 452–458, https://doi.org/10.1107/S2052520614007379.
[28] F. Stern, Elementary theory of the optical properties of solids, Phys. Status Solidi B 15 (1963) 299–408, https://doi.org/10.1016/S0081-1947(08)60594-9.
[29] M. Nowak, B. Kauch, P. Szperlich, Determination of energy band gap of nanocrystalline SbSI using diffuse reflectance spectroscopy, Rev. Sci. Instrum. 80 (2009), 046107, https://doi.org/10.1063/1.3103603.
[30] L. Liu, S. Wang, Z. Yin, et al., Effects of (La, Sr) co-doping on electrical conduction and magnetic properties of BiFeO3nanoparticles, Chin. Phys. B 25 (2016) 0–6, https://doi.org/10.1088/1674-1056/25/9/097801.
[31] J. Varignon, M. Bibes, A. Zunger, Origin of band gaps in 3d perovskite oxides, Nat. Commun. 10 (2019) 1658, https://doi.org/10.1038/s41467-019-09698-6.
[32] C.-C. Hu, C.-C. Tsai, H. Teng, Structure characterization and tuning of perovskite-like NaTaO 3 for applications in photoluminescence and photocatalysis, J. Am.

Ceram. Soc. 92 (2009) 460–466, https://doi.org/10.1111/j.1551-2916.2008.02869.x.
[33] Z.X. Wei, Y. Wang, J.P. Liu, et al., Synthesis, magnetization and photocatalytic activity of LaFeO 3 and LaFe 0.5Mn 0.5-xO 3-δ, Mater. Chem. Phys. 136 (2012) 755–761, https://doi.org/10.1016/j.matchemphys.2012.07.052.
[34] J. Chandradass, A.H. Jadhav, H. Kim, Surfactant modified MgFe2O4nanopowders by reverse micelle processing: effect of water to surfactant ratio (R) on the particle size and magnetic property, Appl. Surf. Sci. 258 (2012) 3315–3320, https://doi.org/10.1016/j.apsusc.2011.11.092.
[35] C. Kursun, M. Gogebakan, E. Uludag, et al., Structural, electrical and magnetic properties of Nd – a – CoO3 (A = Sr, Ca) perovskite powders by mechanical alloying, Sci. Rep. 8 (2018) 13083, https://doi.org/10.1038/s41598-018-31458-7.
[36] C. Cannas, D. Gatteschi, A. Musinu, et al., Structural and magnetic properties of Fe $_2$ O $_3$ nanoparticles dispersed over a silica matrix, J. Phys. Chem. B 102 (1998) 7721–7726, https://doi.org/10.1021/jp981355w.